Shahrood University of Technology
Iranian Society of Mining Engineering (IRSME)
Journal of Mining and Environment (JME)
journal homepage: www.jme.shahroodut.ac.ir
THOMSON REUTERS

Interaction between One Internal Hole and Two Neighboring Joints under Uniaxial Compression using an Experimental Test and a Numerical Simulation

Vahab Sarfarazi[1*], Kaveh Asgari[2], Shadman Mohamadi Bolban Abad[3]

1. Academic Member, Department of Mining Engineering, Hamedan University of Technology, Hamedan, Iran,
2. Research Scholar, Department of Mining Engineering, Shahid Bahonar University of Kerman, Kerman, Iran
3 Research Scholar, Hamedan University of Technology, Hamedan, Iran

Article Info

Received 1 September 2021
Received in Revised form 2 October 2021
Accepted 8 October 2021
Published online 8 October 2021

DOI:10.22044/jme.2021.11157.2095

Keywords

Compressive test
Joint angle
Joint distance
Hole
PFC2D

Abstract

The interaction between an internal hole and two surrounded joints under a uniaxial compression are examined using the experimental and discrete element procedures. Inside the concrete sample, two notches and an internal hole are created. The joint angle change from 0° to 90° with an increment of 30°. The distances between the joint and the internal hole are 2 cm and 3 cm. Also the numerical models are provided. The joint angle change from 0° to 90° with an increment of 15°. The distances between the joint and the internal hole are 2 cm, 3 cm, and 4 cm. The compressive strength is 7.2 MPa. The rate of loading is 0.005 mm/s. The experiment indicates that the failure process is significantly dependent on the notch angle and the joint distance from the hole. The pattern of fracture and mechanism of failure of joints affect the shear strengths of the samples. The models with joint angles of 30° and 60° have a less compressive strength since the pure tensile failure occurs in these configurations. The model strength decreases with decrease in the join spacing. In fact, in the case that the joint spacing is 2 cm, the interaction between the hole and the neighboring joint is so strong. Consequently, the compressive strength is declined. In both approaches of the numerical simulation and experimental methods, the pattern and strength of failure are identical.

1. Introduction

The experimental and *in situ* experiments indicate that the concrete strength can be declined by a porous structure, which can lead to an incompetency of the concrete [1]. Micro-cracks may initiate from the concrete porous structure and integrate together; then they can compose of a fracture plane leading a rock collapse [2-5]. Many researchers have examined the fragile materials with pre-existing defects [6-16]. Diverse kinds of cracks based on their spread mechanism and shape have been identified by Wong and Einstein [14] on plaster and Carrara marble samples with a notch under a uniaxial compression. In addition, they experimentally examined the behavior of specimen cracking with two parallelly open flaws in terms of macroscopic and microscopic under uniaxial compression [9, 10]. Yet, the experimental research works on brittle materials with both circular void and crack are rare. The interactions between a notch and a void in the case that the process of cracking was not assessed and the pore shape was not circular was studied by Kranz [17]. The micromechanics by Lee and Ju [18] represent the interactions between a notch and a pore; yet, the cracking behavior was neglected. Though, some researchers investigated the cracking process of the sample with a hole by uniaxial compression tests [9-12], the impact of pre-existing cracks was ignored. In addition, diverse approaches such as FEM [22-50], BEM [51, 52], DEM [53-56], the numerical manifold method [57], the continuous/discontinuous deformation analysis

Corresponding author: sarfarazi@hut.ac.ir (V. Sarfarazi).

method [58], and the meshless approach [59, 60] have been applied for examining the cracking behavior of brittle materials. From these numerical procedures, DEM is determined as one of the most common approaches for examining the cracking behavior of fragile substances at micro-scale. In addition to that, another popular DEM software is PFC. The principal goal of DEM is to build a material as an assembly of bonded discs based on the law of motion. In this case, the formation of cracks is stimulated between adjacent particles based on the breakage of bonds [61, 62]. The cracking process of fragile materials containing a single [63] and two pre-existing defect(s) [64] under uniaxial loading has been investigate by the particle flow code. Besides, the effect of rate of loading and scale on the cracking process of defected samples under uniaxial compressive loading have been examined [65-75]. In the case that the number and diameter of holes, their center-to-center distances, and the angle between the line connecting the holes and the direction of loading was being changed, Lin *et al*. [76, 77] examined hard rock granite specimens with two holes under a uniaxial compression. Once again, they indicated that tensile, shear, and mixed-mode (shear-tensile) cracks initiated at the hole boundaries during the loading process. Though many researchers examined the impacts of the presence of hole rock and rock-like materials, there is is no study in favour of examining the simultaneous impacts of holes and a notch. In this research work, an experimental test and a PFC2D numerical simulation are used to investigate the interaction between an internal hole and two neighbouring joints under a uniaxial compression.

2. Laboratory Experiments Stages

2.1 Mechanical characteristics of specimens

A mixture of cement and water with a ratio of 2/1 was used to create the specimens. The Brazilian and uniaxial experiments were performed on the cylindrical and disc specimens. The diameter and height of the cylindrical specimens were 54 mm and 108 mm, respectively. In addition, the diameter and thickness of the disc specimens were 54 mm and 27 mm, respectively. Figures 1a and 1b depict the pattern of failure in the uniaxial test and the Brazilian test. Table 1 indicates the compressive and tensile strengths of the rock-like samples.

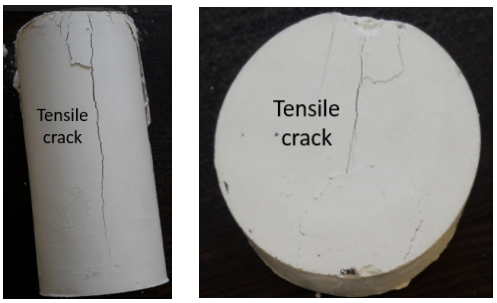

(a) (b)

Figure 1. a) Pattern of failure in experimental the compressive test, b) pattern of failure in the Brazilian test.

Table 1. Mechanical characteristics of the samples.

Uniaxial compressive strength (MPa)	**7.2**
Tensile strength (MPa)	**1.3**

2.2. How to build samples that contain non-persistent joints

For the fabrication of samples containing non-persistent joints and an internal hole, a mixture of cement and water was applied with a ratio of 2/1. The mixtures were inserted in the molds. The dimensions of the framework were 150 mm × 150 mm × 200 mm (Figure 2a). The fiberglass was used for building the model, which did not adsorb water, and consequently, the volume of mold remained constant. A specific plastic fiber with dimensions of 150 mm × 150 mm × 100 mm was placed into the frame (Figures 2a and 2c). Then the aluminum sheets and cylindrical instrument were placed into oil. From one side, it was placed within the plastic fiber, and on the other side, it was attached to the free surface (Figures 2a and 2c). The dimensions of the sheet were 200 mm*20 mm*1 mm, and the diameter of the cylindrical instrument was 20 mm. The bonding between the blade and the chunk was held by oil (Figure 2b). After removing the plaster slurry and spending 15 minutes, the aluminum sheets and the cylindrical instrument were pulled out from the box (Figure 2d). Then the cast bolts were opened (Figure 2c), and the specimens were pulled out from the box (Figure 2d). After 15 days, the specimens were loaded uniaxially, and examined the sample breakage. Generally, the samples with two joints and one internal hole were constructed. The joint angularities changed in four different values, i.e. 0°, 30°, 60° and 90°. The distance between the joint and the internal hole changed in two different values, i.e. 2 cm and 3 cm. Totally, 8 specimens with diverse joint angles and joint spacings were provided.

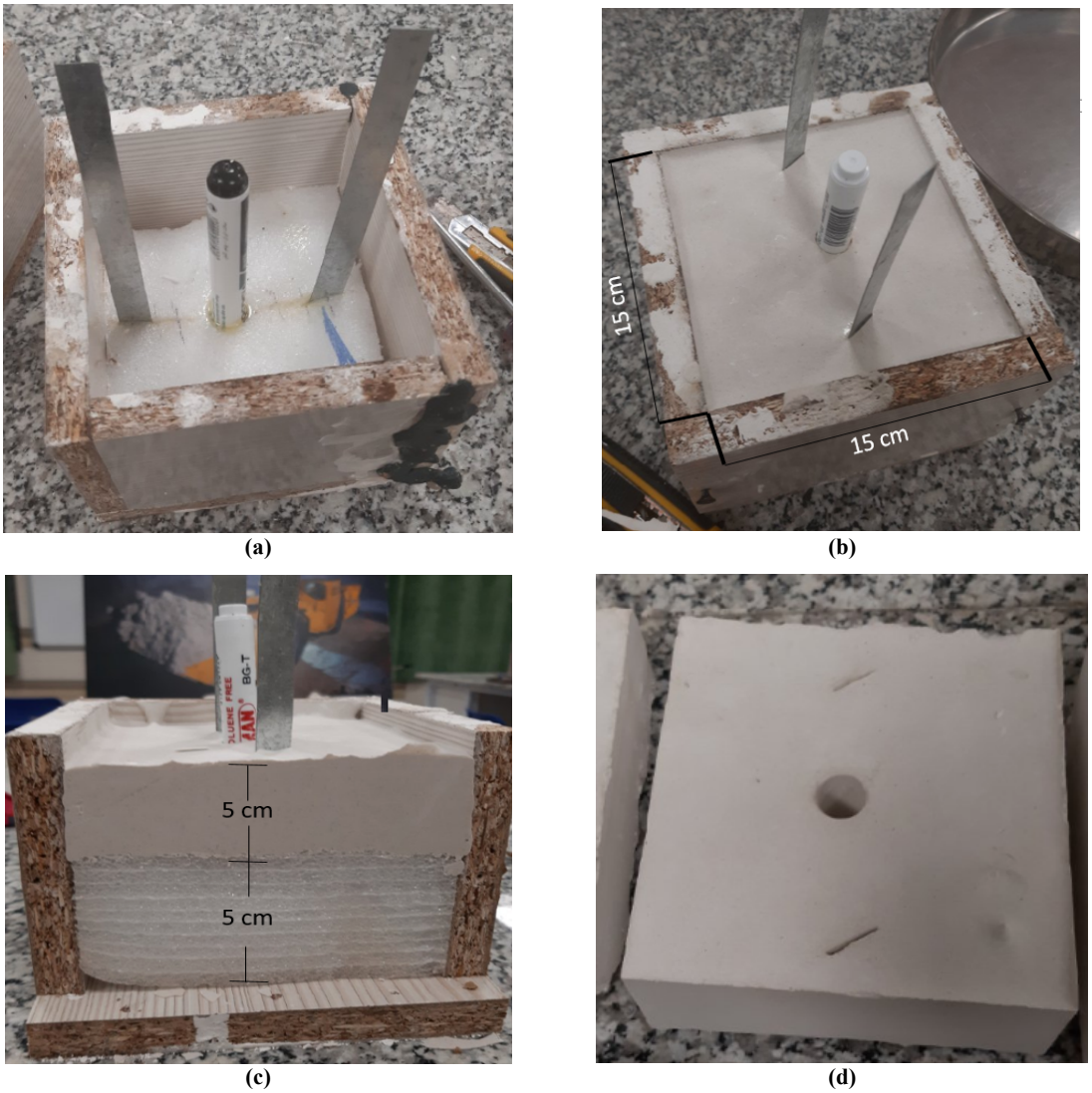

Figure 2. a) Dimensions of frame were 150 mm × 150 mm × 150 mm. A specific plastic fiber with dimensions of 150 mm × 150 mm × 100 mm was placed in the frame, the shim within the plastic fiber, b) the shim adjustment within the frame and plaster slurry inside the mold, c) a sideview of plastic fiber and specimen, D) sample consisting of non-persistent joint and hole.

2.3. Loading sample

In order to perform loading on thev samples, they were situated within the uniaxial machine. The rate of loading was 0.005 mm/s.

3 Experimental results

3.1 Failure mechanism of specimens

a) Distance between joint and internal hole was 2 cm

Figure 3 depicts the pattern of failure of the samples with internal hole and joints with spacing of 2 cm. In the case that the angles of joint were 0° and 30° (Figures 3a and 3b), two outer tensile cracks were initiated from the notch boundaries and spread parallel to the vertical load till coalescence with the specimen. In addition, two inner tensile cracks were initiated from the notch boundaries and spread parallel to the vertical load till coalescence with the hole. In the case that the numbers of joints were 60° and 90° (Figures 3c and 3d), two outer tensile cracks were originated from the notch tips and spread parallel to the vertical load till integrate with boundary of the specimen. In addition, two inner tensile cracks were originated from the notch tips and spread parallel to the loading axis till integrate with the hole.

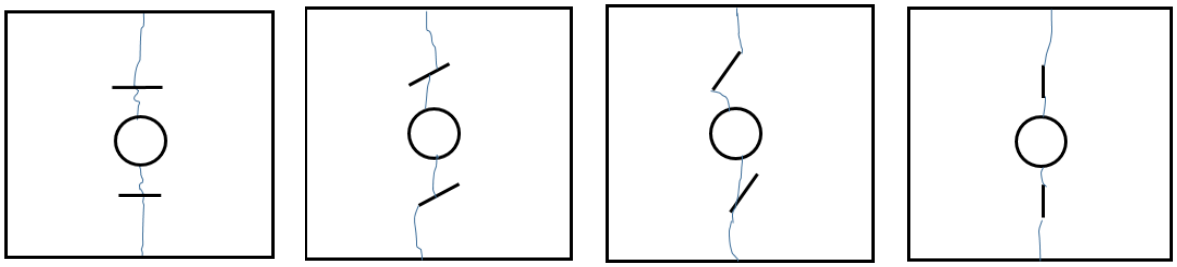

Figure 3. The pattern of failure in sample with joint spacing of 2 cm and diverse joint angle of a) 0˚, b) 30˚, c) 60˚, and d) 90˚.

b) Distance between joint and internal hole was 3 cm

Figure 4 depicts the pattern of failure of samples with internal hole and notches with spacing of 3 cm. In the case that the angles of joint were 0˚ and 30˚ (Figures 4a and 4b), two tensile cracks were originated from the notch and spread parallel to the vertical load until coalescence with the specimen. In addition, two inner tensile cracks were originated from the notch and spread parallel to the vertical load till integrate with the hole. In the case that the numbers of joints were 60˚ and 90˚ (Figures 4c and 4d), two outer tensile cracks were initiated from the notch tips and spread parallel to the vertical load till integrate with the sample boundary. In addition, two inner tensile cracks were initiated from the notch and spread parallel to the vertical load till integrate with the hole. Table 2 shows the places where the new born cracks were initiated.

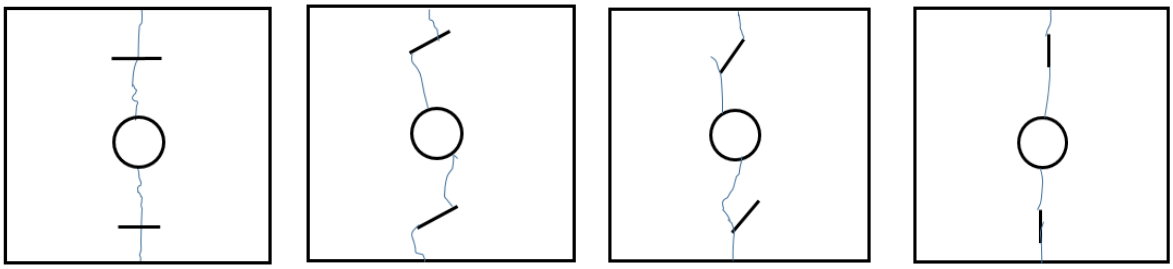

Figure 4. The pattern of failure in sample with joint spacing of 2 cm and various joint angles of a) 0˚, b) 30˚, c) 60˚, and d) 90˚.

Table 2. Crack was initiated from defects.

Distance between joint and internal hole (mm)	Notch angle			
	0	30	60	90
Places where the new born cracks were initiated				
20	Notch wall	Notch wall	Notch tip	Notch tip
30	Notch wall	Notch wall	Notch tip	Notch tip

3.2 Influence of joint angle on specimen strength

Figure 5 indicates the influence of joint angle on the specimen's shear strength for both of the join spacings, i.e. 2 cm and 3 cm. The models with joint angles of 30˚ and 60˚ have a less compressive strength. Also the model strength decreases with decreasing the join spacing. In fact, in the case that the joint spacing was 2 cm, the interaction between the hole and the neighboring joint was so strong. This leads to decreasing the compressive strength.

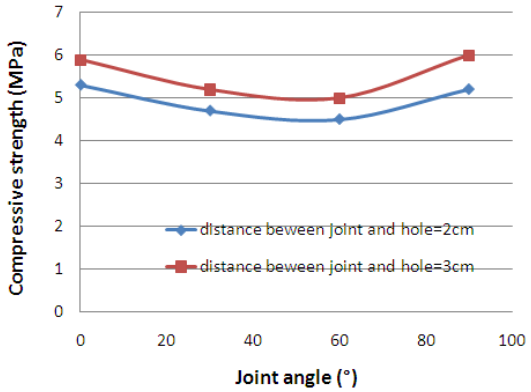

Figure 5. Influence of joint angle on the specimen's compressive strength.

4. Particle Flow Code

PFC2D is a discreet element code that introduces the substance as a solid particles' assembly moving discreetly, and its interaction is just at the contacts (Potyondy and Cundall [64]). This model established an elastic relationship between the relative movements and the particle contact forces. Some provided routines were used for producing a parallel-bonded particle model for PFC2D. In order to produce this model, some micro-characteristics must be introduced such as parallelly-bond stiffness ratio, minimum radius of ball, stiffness ratio kn over ks, ball-to-ball contact modulus, parallelly normal bond strength, coefficient of ball friction, ratio of standard deviation to mean of bond strength both in the normal and shear directions, parallel-bond modulus, parallel shear bond strength, and parallel-bond radius multiplier.

4.1. Preparing and calibrating numerical model

According to the micro-characteristics listed in [57] and calibrating by standard approaches (Potyondy and Cundall, [64]), a calibrated assembly of PFC particle was provided. The dimensions of the uniaxial model were 54 mm and 108 mm. The sample was created by 12,615 particles. The upper and lower walls got closed to each other with a slow rate of 0.016 m/s. The diameter of the Brazilian model was 54 mm. The sample was created by 6421 particles. The surrounding walls got closed to each other with a slow rate of 0.016 m/s. The local damping factor was 0.7 based on the PFC manual. Figures 6a and 6c depict the experimental uniaxial compression test and experimental Brazilian test, respectively. Also Figures 6b and 6d indicate the numerical uniaxial compression test and the numerical Brazilian test, respectively. The results obtained indicate a good matching between the numerical simulation and the experimental test. The uniaxial compression strength, Young modulus, and Brazilian tensile strength are shown in Table 3. These mechanical characteristics are in a good matching with those of the experimental tests (Table 1). This indicates that the calibration of model is correct.

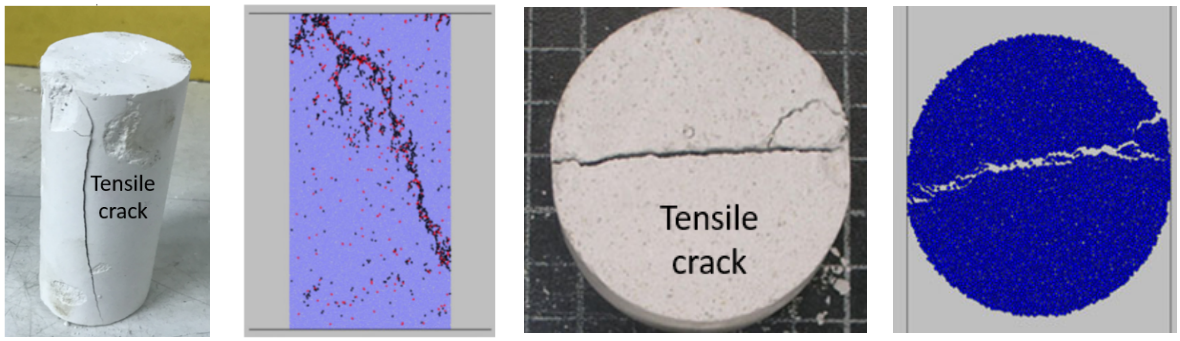

Figure 6. a) Experimental compression test, b) numerical compression test, c) experimental Brazilian test, and d) numerical Brazilian test.

Table 3. Mechanical properties in numerical models.

UCS (MPa)	7.4
Young modulus (GPa)	9.3
Tensile strength (MPa)	1.4

4.2 Numerical compressive tests on non-persistent open joint

The numerical simulation of the compression tests for jointed rocks were performed by making a box model in PFC2D (by applying the calibrated micro-parameters) after calibration of PFC2D (Figures 7-9). The dimensions of the PFC samples were 150 mm × 150 mm. A number of 14321 disks with a minimum radius of 0.27 mm were provided in order to build up the box sample. Two walls were placed at the top and bottom of the model. By elimination of particle bands from the model, the non-persistent joints were made. The notche opening was 1 mm. Also one hole was created in the center of the model. Generally, the models with two joints and one hole were constructed. Generally, the samples containing two joints and one hole were constructed. The joint angularities changed in seven different values, i.e. 0° (Figure 7a), 15° (Figure 7b), 30° (Figure 7c), 45° (Figure 7d), 60° (Figure 7e), 75° (Figure 7f), and 90° (Figure 7g). The distance between the joint and the internal hole changes in two different values, i.e. 2 cm (Figure 7), 3 cm (Figure 8), and 4 cm (Figure 9). Totally, 21 specimen with different joint angles and joint spacings were prepared. It is worthy noting that the joint configuration is similar to the experimental one in 8 various joint configurations, i.e. joint angles of 0°, 30°, 60°, and 90° for the joint spacings of 2 cm and 3 cm. The top and bottom walls induced a uniaxial force on the model. The recorded reaction forces on the top wall were used for registeration of the compression force.

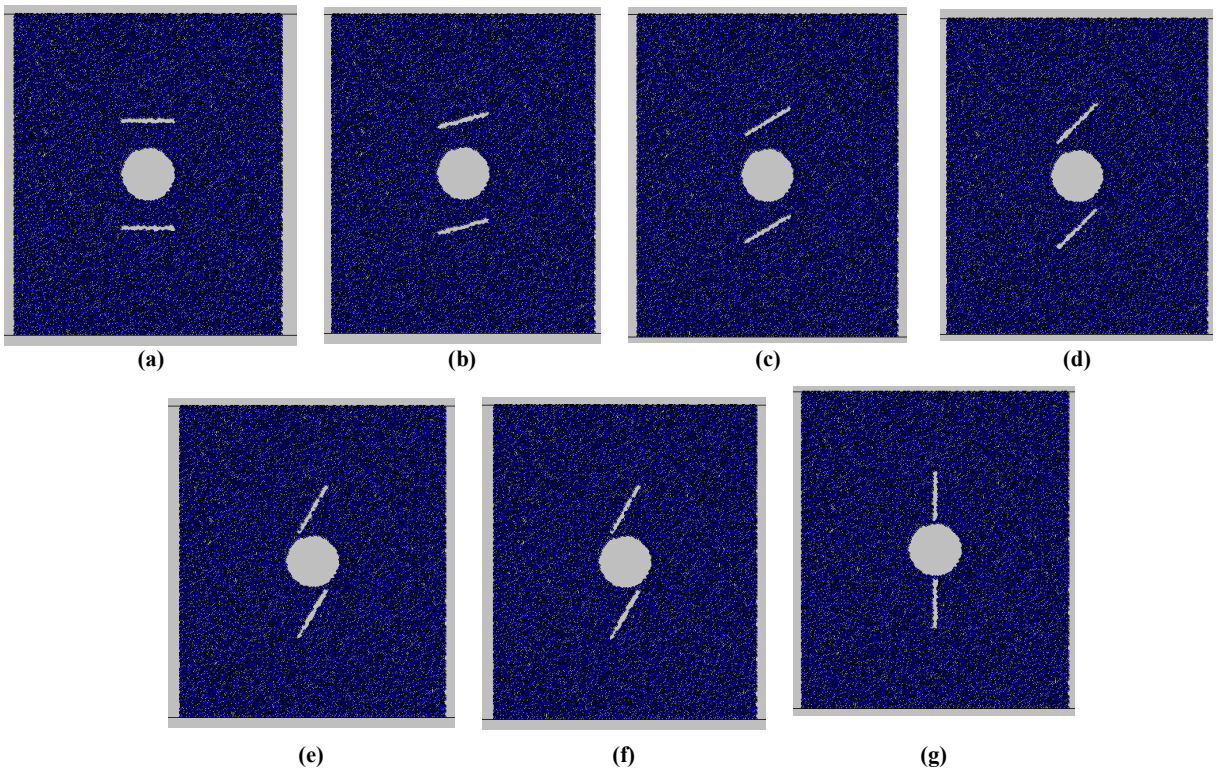

Figure 7. Numerical model with joint angles of a) 0°, b) 15°, c) 30°, d) 45°, e) 60°, f) 75°, and g) 90°.

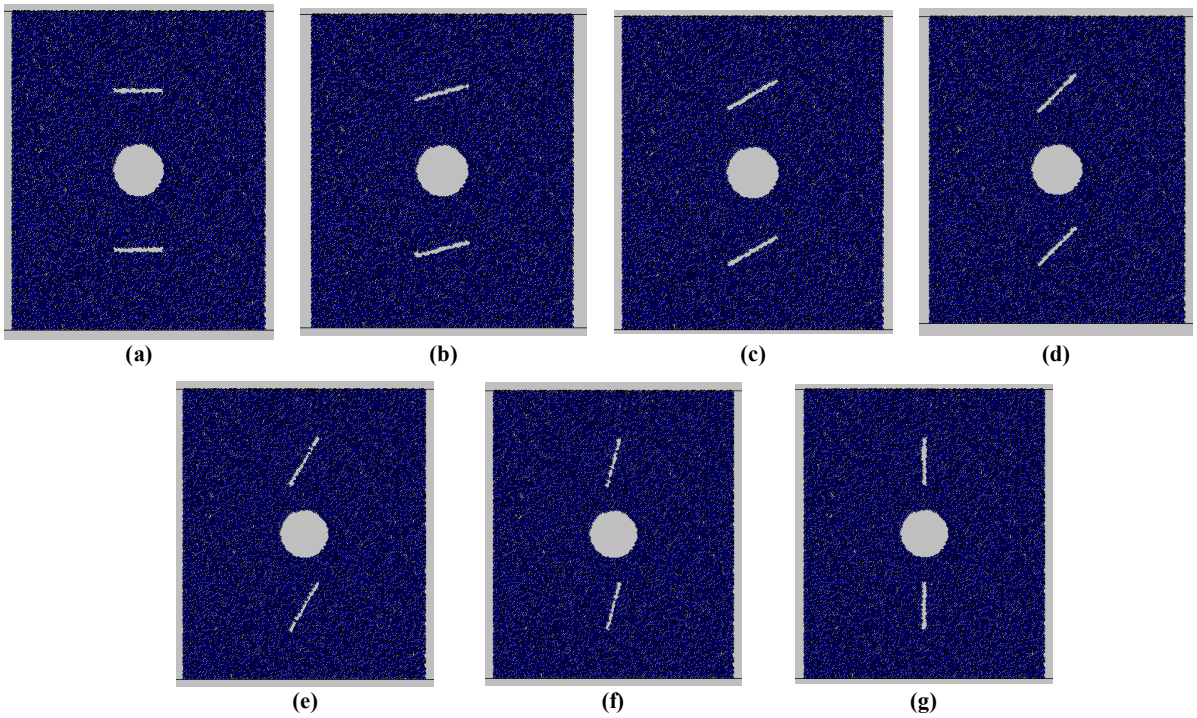

Figure 8. Numerical model with joint angles of a) 0°, b) 15°, c) 30°, d) 45°, e) 60°, f) 75°, and g) 90°.

4.3. Numerical results

4.3.1. Failure mechanism of models

a) Distance between joint and internal hole was 2 cm

Figure 9 indicates the pattern of failure of the samples with an internal hole and a non-persistent joint with a joint spacing of 2 cm. The shear crack is denoted by a red line, while the tensile crack is marked as a black line. In the case that the joint angle was 0° (Figure 10a), two outer tensile cracks were originated from the joint boundaries. The upper tensile fracture grew for a short distance and then stopped but the lower tensile fracture spread parallel to the loading axis till integrate with boundary of the specimen. In addition, two inner tensile cracks were initiated from the joint boundaries and spread parallel to the loading axis till integrate with the hole boundaries. Another tensile fracture was originated from the right tip of the lower joint and spread diagonally till coalescence with boundary of the model. In the case that the angles of joints were 15°, 30°, and 45° (Figures 9b, 9c, and d), two outer tensile cracks were initiated from the joint boundaries. The upper tensile fracture grew for a short distance and then stopped but the lower tensile fracture spread parallel to the loading axis till integrate with the specimen boundary. Further, two inner tensile cracks were initiated from the joint boundaries and spread parallel to the loading axis until integrate with the hole boundaries. Another tensile fracture originated from the right tip of the lower joint and spread diagonally till integrate with the model boundary. This fracture joins the right side of the hole too. In the case that the angles of joints were 60°, 75°, and 90° (Figures 9e, 9f, and 9g), two outer tensile cracks were initiated from the joint boundaries. The upper tensile fracture grew for a short distance and then stopped but the lower tensile fracture spread parallel to the loading axis till integrate with boundary of the specimen. Additionally, two inner tensile cracks were initiated from the joint boundaries and spread parallel to the loading axis till integrate with the hole boundaries. Another tensile fracture was originated from the right side of the hole and propagated diagonally till integrate with the model boundary.

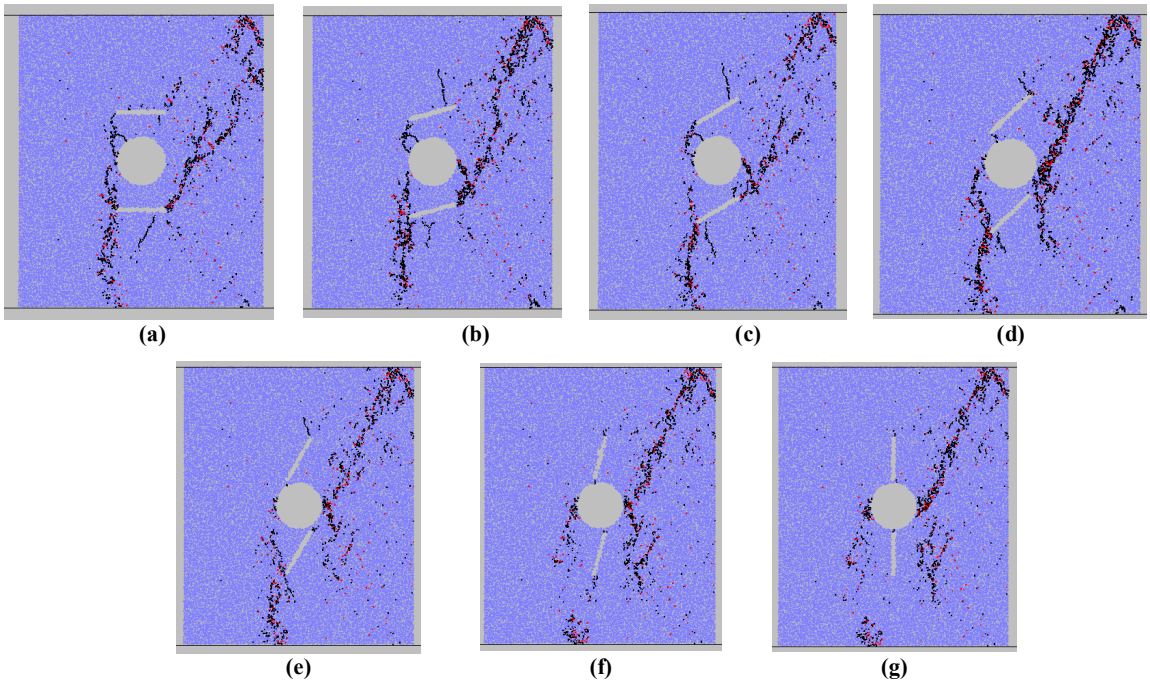

Figure 9. Pattern of failure in numerical model with joint angles of a) 0°, b) 15°, c) 30°, d) 45°,e) 60°, f) 75°, and g) 90°.

b) Distance between joint and internal hole was 3 cm

Figure 10 indicates the pattern of failure of the samples with an internal hole and a non-persistent joint a with joint spacing of 2 cm. The shear crack is denoted by a red line, while the tensile crack is marked as a black line. In the case that the joint angles were 0°, 15°, 30°, and 45° (Figures 10a, 10b, 10c, and 10d), two tensile fractures were originated from the tips of the lower joint. These fractures propagated diagonally till coalescence with boundary of the model.

In the case that the angles of joints werw 60°, 75°, and 90° (Figures 10e, 10f, and 10g), two inner tensile cracks were initiated from the joint tips and spread parallelly to the loading axis till integrate with the boundary of the hole. Also a tensile fracture originated from the right side of the hole and propagated diagonally till integrate with the model boundary.

In the case that the angles of joints were 60°, 75°, and 90° (Figures 12e, 12f, and 12g) the tensile fracture originated from the right side of the hole and propagated diagonally till coalescence with boundary of the model.

By comparing Figures 3 and 4 and Figures 10 and 11, it is deductible that the pattern of failure is approximately identical in both the numerical simulation and the experimental test.

4.4. Influence of joint angles on model's strength

Figure 11 indicates the impact of joint angle on the compressive strength of the models with joint spacings of 2 cm, 3 cm, and 4 cm. The models with joint angles of 30° and 60° have a less compressive strength. Furthermore, the model strength decrease with decreasing the join spacing. In fact, in the case that the joint spacing was 2 cm, the interaction between the hole and the neighboring joint was so strong. This leads to decreasing the compressive strength.

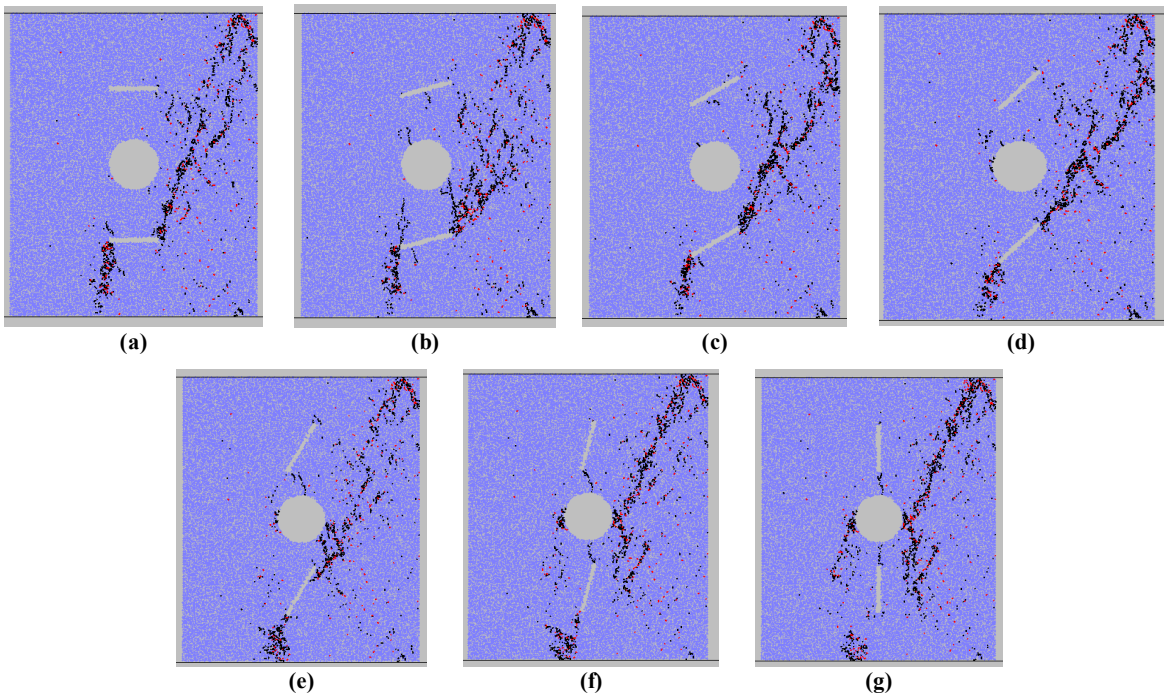

Figure 10. Pattern of failure in numerical model with joint angles of a) 0˚, b) 15˚, c) 30˚, d) 45˚, e) 60˚, f) 75˚, and g) 90˚.

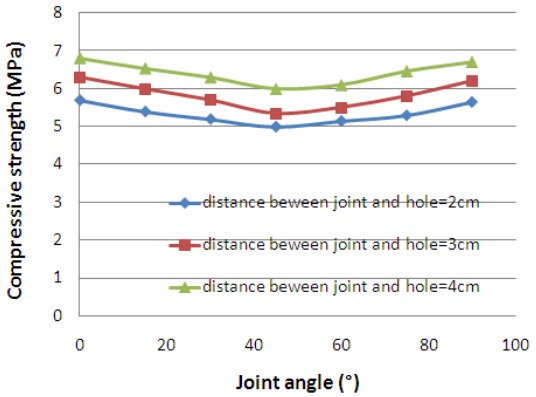

Figure 11. Influence of joint angle on compressive strength of specimens.

By caomparing Figure 5 and Figure 11, it can be indicated that the failure strength is approximately identical in both the numerical simulation and the experimental test.

5. Conclusions

- For a joint spacing of 2 cm, in the case that the joint angle was 0˚, two outer tensile cracks were originated from the joint boundaries. The upper tensile fracture grew for a short distance and then stopped but the lower tensile fracture spread parallel to the loading axis till integrate with the specimen boundaries. In addition, two inner tensile cracks were originated from the boundaries of joint and spread parallel to the loading axis till integrate with boundaries of hole. Another tensile fracture originated from the right tip of the lower joint and spread diagonally till integrate with the model boundary. In the case that the angles of joints were 15˚, 30˚, and 45˚, two outer tensile cracks were initiated from the joint boundaries. The upper tensile fracture grew for a short distance and then stopped but the lower tensile fracture spread parallel to the loading axis till integrate with boundary of the specimen. In addition, two inner tensile cracks were initiated from the joint boundaries and spread parallel to the loading axis till integrate with hole boundaries. Another tensile fracture originated from the right tip of the lower joint and spread diagonally till integrate with the model boundary. This fracture joins the right side of the hole too. In the case that the angles of joints were 60˚, 75˚, and 90˚, two outer tensile cracks were originated from the joint boundaries. The upper tensile fracture grew for a short distance and then stopped but the lower tensile fracture spread parallel to the loading axis till integrate with boundary of the specimen. Also two inner tensile cracks were initiated from the joint boundaries and spread parallel to the loading axis till integrate with the hole boundaries. Another tensile fracture originated from the right side of the hole and propagated diagonally till integrate with the model boundary.

- For a joint spacing of 3 cm, In the case that the joint angles were 0˚, 15˚, 30˚, and 45˚, two tensile fractures originated from the tips of the lower joint. These fractures were propagated diagonally till coalescence with boundary of the model. In the case that the angles of joints were 60˚, 75˚, and 90˚, two inner tensile cracks were originated from the joint tips and spread parallel to the loading axis till integrate with the boundary of the hole. In addition, the tensile fracture originated from the right side of the hole and propagated diagonally till integrate with the model boundary.
- For a joint spacing of 4 cm, in the case that the joint angles were 0˚, 15˚, 30˚, and 45˚, two tensile fractures were originated from the tips of the lower joint. These fractures propagated diagonally till integrate with the model boundary. In the case that the angles of joints were 60˚, 75˚, and 90˚, the tensile fracture was originated from the right side of the hole and propagated diagonally till integrate with the model boundary.
- The models with the joint angles of 30˚ and 60˚ had a less compressive strength since pure tensile failure occurred in these configurations. The failure surface was smooth without a plouverized material. It shows that the tensile failure occurs in these samples. On other hand, the models with joint angles of 0˚ and 90˚ have a more compressive strength since mixed shear/tensile failure occurs in these configurations. Inspection of the failure surface shows that a poluvesrized material exists in the failure surface. It shows that the shear failure occurs in these samples.
- The model strength decreases with decreasing the join spacing. In fact, in the case that the joint spacing was 2 cm, the interaction between the hole and the neighboring joint was so strong. Consequently, the compressive strength was declined.
- The pattern of failure is approximately identical in both the experimental test and the numerical simulation.
- The strength of failure is approximately identical in both the experimental test and the numerical simulation.

References

[1]. Basu, A., Mishra, D.A. (2014). A method for estimating crack-initiation stress of rock materials by porosity. J. Geol. Soc. India., 84 397–405.

[2]. Chang, S. H., Lee, C.I. and Jeon, S. (2002). Measurement of rock fracture toughness under modes I and II and mixed-mode conditions by using disc-type specimens. Eng. Geo., 66: 79-97.

[3]. Hoek, C.D. (2014). Fracture initiation and propagation in intact rock–a revie., J. Rock Mech. Geotech. Eng., 6: 287 –300.

[4]. Lisjak, A. (2017). A 2D, fully coupled, hydro-mechanical, FDEM formulation for modelling fracturing processes in discontinuous, porous rock masses. Comput. Geotech., 8: 1–18.

[5]. Karimpouli, S., Hassani, H., Malehmir, A. (2013). Understanding the fracture role on hydrocarbon accumulation and distribution using seismic data: A case study on a carbonate reservoir from Iran. J. Appl.Geophys., 96: 98–106.

[6]. Bobet, A. and Einstein, H.H. (1998). Fracture integrate in rock-type materials under uniaxial and biaxial compression. Int. J. Rock Mech. Min. Sci., 35: 863–888.

[7]. Wong, R.H.C. (2001). Analysis of crack integrate in rock-like materials containing three flaws-Part I: experimental approach. Int. J. Rock Mech. Min. Sci., 38: 909–924.

[8]. Sagong, M. and Bobet, A. (2002). Integrate of multiple flaws in a rock-model material in uniaxial compression. Int. J. Rock Mech. Min. Sci., 39: 229–241.

[9]. Wong, L.N.Y., and Einstein, H.H. (2009). Crack integrate in molded gypsum and Carrara marble: part 1. Macroscopic observations and interpretation. Rock Mech. Rock Eng., 42: 475–511.

[10]. Wong, L.N.Y. and Einstein, H.H. (2009). Crack integrate in molded gypsum and Carrara marble: part 2-microscopic observations and interpretation. Rock Mech. Rock Eng., 42: 513–545.

[11].Yang, S.Q. (2011). Crack integrate behavior of brittle sandstone samples containing two coplanar fissures in the process of deformation failure. Eng. Fract. Mech., 78: 3059-3081.

[12] .Yang, S.Q. (2008). Experimental investigation on strength and failure behavior of pre-cracked marble under conventional triaxial compression. Int. J. Solids Struct., 45: 4796–4819.

[13]. Yang, S.Q., (2012). An experimental study of the fracture integrate behaviour of brittle sandstone specimens containing three fissures. Rock Mech. Rock Eng., 45: 563–582.

[14]. Wong, L.N.Y. and Einstein, H.H. (2009). Systematic evaluation of cracking behavior in specimens containing single flaws under uniaxial compression. Int. J. Rock Mech. Min. Sci., 46: 239–249.

[15]. Park, C.H. and Bobet, A. (2010). Crack initiation, propagation and integrate from frictional flaws in uniaxial compression. Eng. Fract. Mech., 77: 2727–2748.

[16]. Park, C.H. and Bobet, A. (2009). Crack integrate in specimens with open and closed flaws: a comparison. Int. J. Rock Mech. Min. Sci., 46: 819–829.

[17] Kranz, R.L. (1979). Crack-crack and crack-pore interactions in stressed granite. Int. J. Rock Mech. Min. Sci., 16: 37–47.

[18]. Lee, H.K. and Ju, J.W. (2007). A 3D stress analysis of a penny-shaped crack interacting with a spherical inclusion. Int. J. Damage Mech., 16: 331–359.

[19]. Carter, B.J. (1992). Size and stress gradient effects on fracture around cavities. Rock Mech. Rock Eng., 25:167–186.

[20]. Carter, B.J., (1991). Primary and remote fracture around underground cavities. Int. J. Numer. Anal. Methods Geomech., 15P:1–40.

[21]. Wong, R.H.C. (2006). Experimental and numerical study on splitting failure of brittle solids containing single pore under uniaxial compression., Mech. Mater., 38: 142–159.

[22]. Bocca, P. , Carpinteri, A. and Valente, S. (1990). Size effects in the mixed mode crack propagation: softening and snap-back analysis. Eng. Fract. Mech., 35:159-170.

[23] Xu, C. and Fowell, R.J. (1994). Stress intensity factor evaluation for cracked chevron notched Brazilian disc specimens. Int. J. Rock Mech. Min. Sci., 31: 157–162.

[24]. Trädegård, A. (1998). FEM-remeshing technique applied to crack growth problems. Comput. Methods Appl. Mech. Eng., 160:115–131.

[25]. Barani, O.R. , Khoei, A.R. and Mofid, M. (2011). Modeling of cohesive crack growth in partially saturated porous media; a study on the permeability of cohesive fracture. Int. J. Fract., 167: 15– 31.

[26]. Tan, X. H. (2015). A simulation method for permeability of porous media based on multiple fractal model. Int. J. Eng. Sci., 95: 76-84.

[27].Ţene, M., (2016). Algebraic multiscale method for flow in heterogeneous porous media with embedded discrete fractures. J. Comput. Phys., 321: 819 –845.

[28]. Supar, K. and Ahmad, H. (2017). XFEM modelling of multi-holes plate with single-row and staggered holes confi gurations. MATEC Web Conf. 103, 02031.

[29]. Schrefler, B.A. and Xiaoyong, Z. (1993). A fully coupled model for water flow and air flow in deformable porous media. Water Res. Res., 29: 155 –167.

[30]. Aliha, M.R. (2012). Mixed mode I/II fracture path simulation in a typical jointed rock slope. 4th Int. Conf. Crack Paths, pp:55-60.

[31]. Sukumar, N. (2001). Modeling holes and inclusions by level sets in the extended finite-element method. Comput. Meth. Appl. Mech. Eng,. 190: 6183-6200.

[32] . Gordeliy, E. and Peirce, A. (2015). Enrichment strategies and convergence properties of the XFEM for hydraulic fracture problems. Comput. Methods Appl. Mech. Eng., 283: 474-502.

[33]. Mohammadnejad, T. (2013). An extended fi nite element method for hydraulic fracture propagation in deformable porous media with the cohesive crack mode. Finite Elem. Anal. Des., 73: 77 –95.

[34]. Khoei, A.R., (2014). A mesh-independent finite element formulation for modeling crack growth in saturated porous media based on an enriched-FEM technique. Int. J. Fract., 188: 79 –108.

[35]. Gordeliy, E. and Peirce, A. (2013). Coupling schemes for modeling hydraulic fracture propagation using the XFEM. Comput. Meth. Appl. Mech. Eng., 253: 305 –322.

[36]. Dahi-Taleghani, A. and Olson, J.E. (2011). Numerical modeling of multistranded-hydraulic-fracture propagation: accounting for the interaction between induced and natural fractures. SPE J., 16: 575 –581.

[37]. Réthoré, M.A. (2007). A two-scale approach for fluid fl A t fractured porous media. Int. J. Numer. Meth. Eng., 71: 780 – 800.

[38] T.P. Cheng and K.W. Fries, Higher-orderXFEM for curved strong and weak dis-continuities, Int. J. Numer. Meth. Eng. 82 (2010) 564 –590.

[39] S. Mohammadi, XFEM Fracture Analysis of Composites, John Wiley & Sons Incorporated, 2012,

[40]. Natarajan, S., Roy Mahapatra, D. and Bordas, S.P.a. (2010). Integrating strong and weak dis continuities without integration subcells and example applications in an XFEM/ GFEM framework. Int. J. Numer. Methods Eng., 83: 269 –294.

[41] .Wong, L.N.Y. and Einstein, H.H. (2009). Crack integrate in molded gypsum and carrara marble: part 1. Macroscopic observations and interpretation. Rock Mech. Rock Eng,. 42: 475-511.

[42]. Wong, L.N.Y. and Einstein, H.H. (2009). Crack integrate in molded gypsum and carrara marble: Part 2 – Microscopic observations and interpretation. Rock Mech. Rock Eng., 42: 513 –545.

[43]. Ju, Y. (2008). A statistical model for porous structure of rocks. Sci. China, Ser. E Technol. Sci., 51: 2040 –2058.

[44]. Hedjazi, L. (2012). Application of the discrete element method to crack propagation and crack branching in a vitreous dense biopolymer material. Int. J. Solids Struct., 49:1893 –1899.

[45]. Vahab, M. and Khalili, N.(2018). X-FEM modeling of multizone hydraulic fracturing treatments

within saturated porous media. Rock Mech. Rock Eng., 51: 3219 –3239.

[46]. Haddad, M. and Sepehrnoori, K. (2016). XFEM-Based CZM for the simulation of 3D multiple-cluster hydraulic fracturing in quasi-brittle shale formations. Rock Mech. Rock Eng, 49: 4731-4748.

[47]. Natarajan, S. (2011). Enriched finite element methods: advances and applications.

[48]. Rodriguez-Florez, N. (2017). The use of XFEM to assess the in fluence of intra-cortical porosity on crack propagation. Comput. Meth. Biomech. Biomed. Eng., 20: 385–392.

[49]. Florez R. (2018). Mechanics of Cortical Bone: Exploring the Micro- and Nano-Scale, Imperial College London.

[50]. Bouchard, P.O., Bay, F. and Chastel, Y. (2003). Numerical modelling of crack propagation: automatic remeshing and comparison of different criteria. Comput. Methods Appl. Mech. Eng., 192: 887–3908.

[51]. Li, H. and Wong, L.N.Y. (2012). Influence of flaw inclination angle and loading condition on crack initiation and propagation. Int. J. Solids Struct., 49: 2482–2499.

[52]. Bobet, A. and Einstein, H.H. (1998). Numerical modeling of fracture integrate in a model rock material. Int. J. Fract., 92: 221–252.

[53]. Hosseini-Tehrani, P. (2005). Boundary element analysis of stress intensity factor KI in some two-dimensional dynamic thermoelastic problems. Eng. Anal. Boundary Elem., 29: 232–240.

[54]. Lu, X. and Wu, W.L. (2006). A sub-region DRBEM formulation for the dynamic analysis of 2D cracks. Math. Comput. Model., 43: 76–88.

[55]. Zhang, X.P. and Wong, L.N.Y. (2013). Crack initiation, propagation and integrate in rock-like material containing two flaws: a numerical study based on bonded-particle model approach. Rock Mech. Rock Eng., 46: 1001–1021.

[56]. Ghazvinian, A., Sarfarazi, V. (2012). A study of the failure mechanism of planar non-persistent open joints using PFC2D. Rock Mech.Rock Eng., 45: 677–693.

[57]. Sarfarazi, V. (2014). Numerical simulation of the process of fracture of echelon rock joints. Rock Mech. Rock Eng., 47: 1355–1371.

[58]. Park, J.W. and Song, J.J. (2009). Numerical simulation of a direct shear test on a rock joint using a bonded-particle model. Int. J. Rock Mech. Min. Sci., 46:1315–1328.

[59]. Wu, Z. and Wong, L.N.Y. (2012). Frictional crack initiation and propagation analysis using the numerical manifold method. Comput. Geotech., 39: 38–53.

[60]. Cai, Y.C. (2013). A continuous/discontinuous deformation analysis (CDDA) method based on deformable blocks for fracture modeling. Front. Struct. Civ. Eng., 7: 369–378.

[61]. Zhuang, X.Y. and Augarde, C. (2010). Aspects of the use of orthogonal basis functions in the element-free Galerkin method. Int. J. Numer. Meth. Eng., 81: 366–380.

[62]. Zhu, H.H. (2011). High rock slope stability analysis using the enriched meshless shepard and least squares method. Int. J. Comput. Methods, 8: 209-228.

[63. Itasca, (2004). PFC2D (Particle Flow Code in 2 Dimensions), Version 3.1 Minneapolis.

[64]. Potyondy, D.O. and Cundall, P.A. (2004). A bonded-particle model for rock. Int. J. Rock Mech. Min. Sci., 41: 1329–1364.

[65]. Zhang, X.P. and Wong, L.N.Y. (2012). Cracking processes in rock-like material containing a single flaw under uniaxial compression: a numerical study based on parallelly bonded-particle model approach. Rock Mech. Rock Eng., 45: 711–737.

[66] Lee, H. and Jeon, S. (2011) An experimental and numerical study of fracture integrate in pre cracked specimens under uniaxial compression. Int. J. Solids Struct., 48: 979-999.

[67]. Uzun Yaylacı, E., Yaylacı, M., Ölmez, H., and Birinci, A. (2020). Artificial Neural Network Calculations for A Receding Contact Problem. Computers and Concrete, 2(6): 88-99.

[68]. Yaylacı, M., Eyüboğlu, A., Adıyaman, G., Uzun Yaylacı, E., Öner, E., and Birinci, A. (2021). ssessment of different solution methods for receding contact problems in functionally graded layered mediums. Mechanics of Materials, 33(2): 99-111.

[69]. Yaylacı, M., Yaylı M., Uzun Yaylacı E., Ölmez, H., and Birinci A. (2021). Analyzing the contact problem of a functionally graded layer resting on an elastic half plane with theory of elasticity, finite element method and multilayer perceptron. Structural Engineering and Mechanics, 78(5): 585-597.

[70]. Yaylaci, M. (2016). The investigation crack problem through numerical analysis. Structural Engineering and Mechanics, 57(6): 1143-1156.

[71]. Haeri, H. and Marji, MF. (2016). Simulating the crack propagation and cracks coalescence underneath TBM disc cutters. Arabian Journal of Geosciences, 9 (2):124-130.

[72]. Lak, M., Marji, M.F. (2019). Discrete element modeling of explosion-induced fracture extension in jointed rock masses. Journal of Mining and Environment, 10 (1): 125-138.

[73]. Yavari, MD. (2021). On the propagation mechanism of cracks emanating from two neighboring holes in cubic concrete specimens under various lateral

confinements. Journal of Mining and Environment (accepted for publication).

[74]. Abdollahipour, A. and Marji, MF. (2020). A thermo-hydromechanical displacement discontinuity method to model fractures in high-pressure, high-temperature environments. Renewable Energy, 153: 1488-1503.

[75]. Bakhshi, E. (2019). Hydraulic Fracture Propagation: Analytical Solutions versus Lattice Simulations. Journal of Mining and Environment, 10 (2): 451-464.

[76]. Lin, P., (2015). Experimental study of coalescencemechanisms and failure under uniaxial compression of granitecontaining multiple holes. Int J Rock Mech Min Sci., 77:557-582.

[77]. Lin, Q., (2020). Mechanical behavior around double circular openings in a jointed rock mass under uniaxial compression. Archives of Civil and Mechanical Engineering, 20(1):19-29.

اندرکنش بین حفره و دو ترک مجاور تحت آزمایش تک محوره با استفاده از آزمون آزمایشگاهی و شبیه سازی عددی

وهاب سرفرازی[1*]، کاوه عسگری[2] و شادمان محمدی بلبان آباد[3]

۱- بخش مهندسی معدن، دانشگاه صنعتی همدان، همدان، ایران
۲ بخش مهندسی معدن، دانشگاه شهید باهنر کرمان، کرمان، ایران
۳- بخش مهندسی معدن، دانشگاه صنعتی همدان، همدان، ایران

ارسال ۲۰۲۱/۰۹/۰۱، پذیرش ۲۰۲۱/۱۰/۰۸

* نویسنده مسئول مکاتبات: sarfarazi@hut.ac.ir

چکیده:

در این مقاله، اندرکنش بین یک خفره و دو ترک مجاور درون نمونه بتنی تحت بار تک محوره با استفاده از آزمون آزمایشگاهی و شبیه سازی عددی بررسی شده است. زاویه ترک از صفر درجه تا ۹۰ درجه با گامهای ۳۰ تغییر می کند. فاصله بین ترک و حفره ۲ و ۳ سانتیمتر است. همزمان با تست آزمایشگاهی، مدلسازی عددی نیز انجام شد.. در مدل های عددی، زاویه ترک از صفر درجه تا ۹۰ درجه با گامهای ۱۵ تغییر می کند . مقاومت تک محوره نمونه بکر ۷/۲ مگاپاسکال است. نرخ بارگذاری ۰/۰۰۵ میلیمتر بر ثانیه است. نتایج نشان دادند که الگوی شکست تابع زاویه ترک و فاصله از خفرا است. الگوی شکست و مکانیزم شکست مقاومت فشـــاری نمونه را تحت تاثیر قرار می دهند. مدلهایی با زاویه ترک ۳۰ درجه و ۶۰ درجه کمترین مقاومت را دارند زیرا ترک کشـــشـــی در این مدل ها بوقوع می پیوندد. با کاهش فاصـــله ترک از حفره، مقاومت نمونه کاش می یابد. درحقیقت زمانیکه فاصـــله ترک از حفره ۲ ســـانتیمتر اســـت، اندرکنش بین حفره و ترک زیاد است که منحر به کاهش مقاوم می گردد. الگوی شکست و مقاوم شکست مدل های عددی و نمونه های آزمایشگاهی تقریبا یکسان است.

کلمات کلیدی: آزمایش فشاری، زاویه ترک، فاصله داری ترک، حفره، PFC.